nature physics

ARTICLES

PUBLISHED ONLINE: 25 JANUARY 2016 | DOI: 10.1038/NPHYS3629

Double-Q spin-density wave in iron arsenide superconductors

J. M. Allred[1]*, K. M. Taddei[1,2], D. E. Bugaris[1], M. J. Krogstad[1,2], S. H. Lapidus[3], D. Y. Chung[1], H. Claus[1], M. G. Kanatzidis[1,4], D. E. Brown[2], J. Kang[5], R. M. Fernandes[5], I. Eremin[6,7], S. Rosenkranz[1], O. Chmaissem[1,2] and R. Osborn[1]

Elucidating the nature of the magnetic ground state of iron-based superconductors is of paramount importance in unveiling the mechanism behind their high-temperature superconductivity. Until recently, it was thought that superconductivity emerges only from an orthorhombic antiferromagnetic stripe phase, which can in principle be described in terms of either localized or itinerant spins. However, we recently reported that tetragonal symmetry is restored inside the magnetically ordered state of certain hole-doped compounds, revealing the existence of a new magnetic phase at compositions close to the onset of superconductivity. Here, we present Mössbauer data that show that half of the iron sites in this tetragonal phase are non-magnetic, establishing conclusively the existence of a novel magnetic ground state with a non-uniform magnetization that is inconsistent with localized spins. Instead, this state is naturally explained as the interference between two commensurate spin-density waves, a rare example of collinear double-Q magnetic order. Our results demonstrate the itinerant character of the magnetism of the iron pnictides, and the primary role played by magnetic degrees of freedom in determining their phase diagram.

One of the earliest debates in correlated electron physics was whether a theory of magnetism in ferromagnetic transition metals, such as iron and nickel, should start by treating the electrons as localized in 3*d* orbitals, interacting through Heisenberg exchange interactions, or as itinerant electrons in exchange-split bands[1–3]. It took nearly fifty years to reconcile evidence for both viewpoints through the development of theories of itinerant electron spin fluctuations[4]. This dichotomy between real space and reciprocal space approaches to describing strong electron correlations is at the heart of many problems in condensed matter physics.

A contemporary example is the iron-based superconductors, which are metals whose superconductivity occurs in proximity to a magnetic instability. Because this suggests that magnetic fluctuations could play a key role in promoting superconducting order[5,6], it is important to establish the nature of the magnetism in these materials, but experimental results have been invoked to support both localized-spin approaches and itinerant models.

On the one hand, the large resistivities and enhanced effective masses of the iron arsenides and chalcogenides have been interpreted as evidence for proximity to a Mott transition, as seen in the similar phase diagrams of cuprate superconductors[7–9]. This favours an approach based on localized-spin models, in which the iron spins $\mathbf{S}_i$, with fixed amplitude M, live on the sites i of the iron lattice and interact with each other via interionic exchange interactions. This can give rise to superconductivity with extended *s*-wave symmetry, in which the order parameter changes sign between next-nearest neighbour sites. Some localized models focus not on magnetic, but on orbital degrees of freedom, whose fluctuations in general favour a uniform *s*-wave state[10,11]. In this case, magnetic order is a secondary effect of the four-fold symmetry breaking produced by changing the relative occupations of the d_{xz} and d_{yz} iron orbitals.

On the other hand, the metallic character of these compounds and the quasi-nesting features of their Fermi surfaces have been invoked in favour of an itinerant scenario[12–14]. In this case, instead of local spins on the lattice sites, the magnetism is best described as a modulation of the spin polarization of the itinerant electrons, that is, a spin-density wave, $\mathbf{S}(\mathbf{r}) = \mathbf{M}\cos(\mathbf{Q}\cdot\mathbf{r})$, where $\mathbf{Q}$ is the nesting wavevector, usually either $(\pi, 0)$ or $(0, \pi)$ in these compounds. The resulting superconducting symmetry depends on details of the Fermi surface, and is usually extended *s*-wave, but can also be *d*-wave.

Determining which approach provides the most suitable starting point to model the magnetic interactions of the iron pnictides—itinerant or localized—will therefore have profound consequences both for the nature of the emergent superconductivity and for its relation to cuprate superconductivity[15]. In this paper, we present experimental evidence that the magnetism in these materials is not consistent with a purely localized model of magnetic moments with fixed length, but can be naturally explained in terms of itinerant spin-density waves. Itinerancy here does not imply weak electron correlations, but rather that the spins cannot be localized at the lattice sites and that their amplitudes are not fixed (that is, longitudinal fluctuations are important). It is known that at least moderate electron interactions are essential to describe the full magnetic spectrum of these materials[16–21], but our results show

[1]Materials Science Division, Argonne National Laboratory, Argonne, Illinois 60439, USA. [2]Physics Department, Northern Illinois University, DeKalb, Illinois 60115, USA. [3]Advanced Photon Source, Argonne National Laboratory, Argonne, Illinois 60439, USA. [4]Department of Chemistry, Northwestern University, Evanston, Illinois 60208, USA. [5]School of Physics and Astronomy, University of Minnesota, Minneapolis, Minnesota 55455, USA. [6]Institut für Theoretische Physik III, Ruhr-Universität Bochum, 44801 Bochum, Germany. [7]National University of Science and Technology MISiS, 119049 Moscow, Russia. *e-mail: jmallred@ua.edu

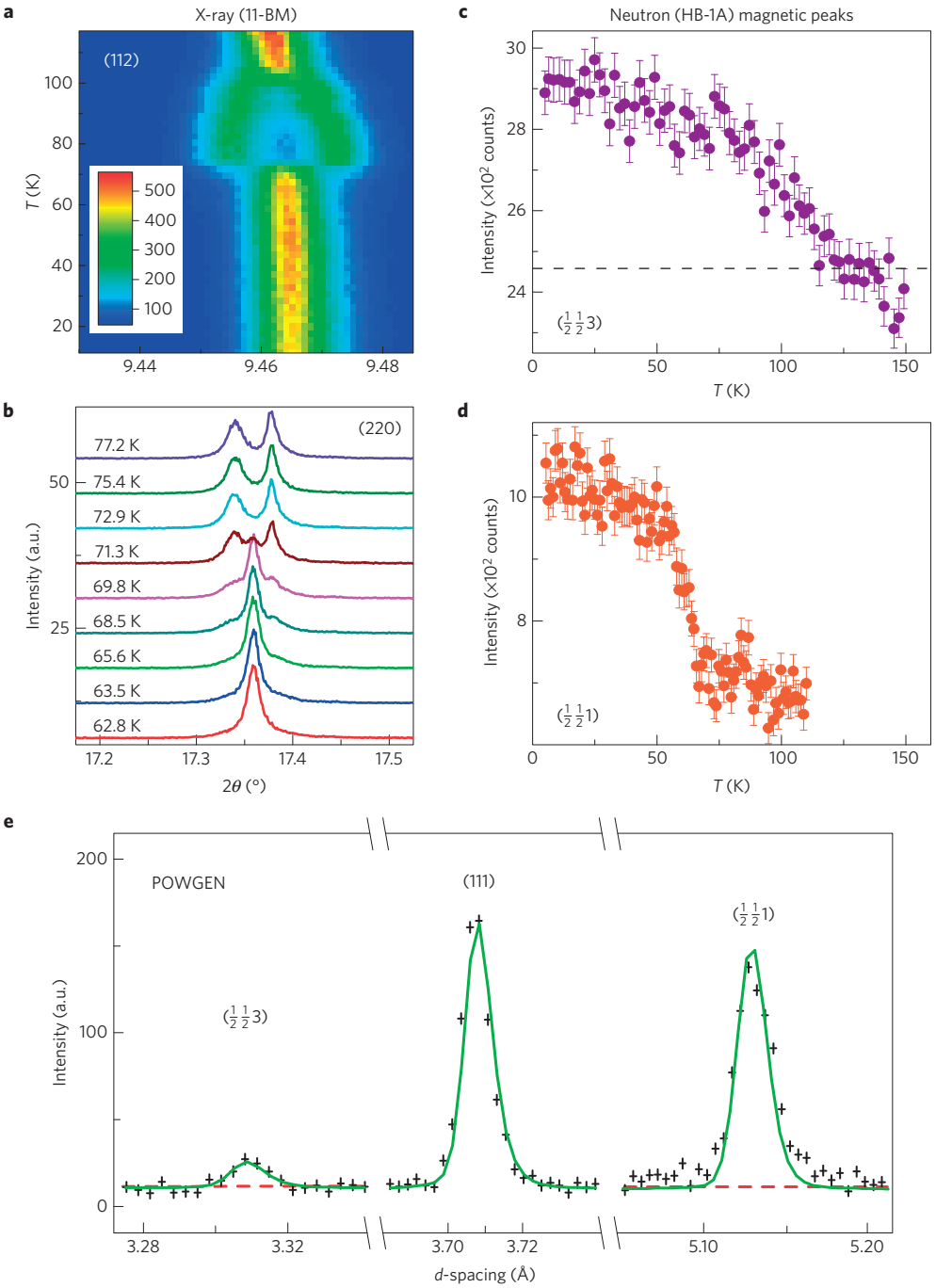

Figure 1 | Temperature-dependent diffraction data of $Sr_{0.63}Na_{0.37}Fe_2As_2$. a,b, X-ray data (11-BM, $\lambda = 0.413842$ Å). **a**, False colour map of the data around the tetragonal (112) peak. **b**, View of the tetragonal (220) peak at temperatures near T_r taken from the same data. **c,d**, Data from constant wavelength neutrons (HB-1A, $\lambda = 2.3626$ Å) showing the intensity of the $(\frac{1}{2}\frac{1}{2}3)$ and $(\frac{1}{2}\frac{1}{2}1)$ magnetic peaks, respectively. **e**, Detailed view of the calculated intensity (green line) from the magnetic model fit to the 10 K POWGEN data (black crosses). The dashed red line shows the calculated intensities of a non-magnetic model. The error bars of the neutron diffraction data are determined from the Poisson statistics of the raw counts.

that the magnetism should be viewed as modulations of the spin polarization in correlated bands rather than as localized spins.

Our conclusions follow from the direct observation of a collinear tetragonal double-**Q** magnetic phase in $Sr_{1-x}Na_xFe_2As_2$ ($x = 0.37$), in which the magnetization is spatially non-uniform. This phase is equivalent to the so-called C_4 magnetic phase recently reported in the closely related compounds, $Ba_{1-x}Na_xFe_2As_2$, with $0.24 \leq x \leq 0.28$ (refs 22,23). In most of the iron-based superconductors, the iron atoms in each plane sit on a square lattice and the antiferromagnetic state usually consists of stripes of in-plane iron spins aligned ferromagnetically along one iron–iron bond direction and antiferromagnetically along the other, with a two-fold (C_2) symmetry that breaks the four-fold (C_4) symmetry of the paramagnetic phase below a coupled magnetic-structural transition at a temperature T_N (refs 15,19,21,24). However, in these hole-doped compounds, four-fold symmetry is restored inside the magnetically ordered state at T_r ($T_r < T_N$). Because the magnetic Bragg peaks have the same reciprocal lattice indices above and below T_r, the C_4 phase was previously interpreted as a double-**Q** magnetic structure described by a coherent superposition of

two spin-density waves, $\mathbf{S}(\mathbf{r}) = \mathbf{M}_1 \cos(\mathbf{Q}_1 \cdot \mathbf{r}) + \mathbf{M}_2 \cos(\mathbf{Q}_2 \cdot \mathbf{r})$, with $\mathbf{Q}_1 = (\pi, 0)$, $\mathbf{Q}_2 = (0, \pi)$, and $|\mathbf{M}_1| = |\mathbf{M}_2|$, which restores four-fold symmetry. Three compounds within the AFe_2As_2 series (A = Ba, Sr) have now shown signatures of this C_4 phase, indicating that it is a universal feature of hole-doping[23,25–27].

Our work provides a significant advance over the earlier results. Previously, evidence for the double-**Q** phase was indirect, relying on the absence of a detectable orthorhombic distortion in the X-ray diffraction. As pointed out in ref. 28, the spin reorientation combined with other types of orbital order could account for a sudden decrease of the orthorhombic distortion below the resolution limit, without the need to invoke a double-**Q** configuration. Furthermore, the earlier measurements could not distinguish between the two possible types of double-**Q** structure, where the two components are either non-collinear ($\mathbf{M}_1$ and $\mathbf{M}_2$ perpendicular) or collinear ($\mathbf{M}_1$ and $\mathbf{M}_2$ parallel)[23,29–34]. The distinction between them is fundamental: whereas in a non-collinear phase, the amplitudes of the spins at the Fe sites are the same (and therefore compatible with a local-moment description), in a collinear phase, the spin amplitudes at the Fe sites are non-uniform, vanishing on half of the sites and doubling on the others.

We have now utilized Mössbauer spectroscopy as a local probe of the magnetization on the ^{57}Fe sites to overcome these limitations. Below T_N, within the C_2 phase, we find that all sites show the same Zeeman splitting due to internal molecular fields, as expected for single-**Q** stripes. However, below the C_4 transition at T_r, we observe that 50% of the iron sites are non-magnetic, whereas the other 50% show an exact doubling of the magnetization, providing unambiguous evidence of collinear double-**Q** magnetic order that is consistent with a reorientation of the magnetic moments along the c-axis[35].

This double-**Q** order is a remarkable manifestation of the difference between localized and itinerant magnetism. Non-collinear multiple-**Q** spin-density waves have been observed in itinerant magnets such as doped γ-manganese[36–38]. What makes our current observation unique is that the superposition of the two single-**Q** modulations is collinear, leading to both constructive and destructive interference of the spin-density waves on alternate sites, $\mathbf{S}(\mathbf{r}) = \mathbf{M} \cos(\mathbf{Q}_1 \cdot \mathbf{r}) + \mathbf{M} \cos(\mathbf{Q}_2 \cdot \mathbf{r})$. Although non-magnetic sites could, in principle, result from strong frustration in a localized model, the precise doubling of the magnetic moments on the remaining magnetic sites indicates a redistribution of the spin density that is incompatible with localized spins but demonstrates conclusively the itinerant character of the magnetism in these iron pnictides.

Results

X-ray and neutron diffraction. Magnetism in the hole-doped series, $Sr_{1-x}Na_xFe_2As_2$, has higher transition temperatures and persists to higher levels of sodium concentration than the equivalent barium series[22,39]. We synthesized a compound with the nominal composition of $Sr_{0.63}Na_{0.37}Fe_2As_2$, below the critical phase boundary for magnetic order, which has a superconducting transition at 12 K. Rietveld refinements of the X-ray powder diffraction spectra yielded a sodium concentration of $x = 0.3691(5)$. More details of the sample characterization are provided in Methods and the Supplementary Information.

The transition from tetragonal ($I4/mmm$) to orthorhombic ($Fmmm$) symmetry is evident in the powder X-ray diffraction as a splitting of some of the Bragg peaks, such as the (112) peak, shown in Fig. 1a. This C_2 transition, which is either weakly first order or second order, occurs around $T_N \approx 105(2)$ K, below which the orthorhombic order parameter (that is, the magnitude of peak splitting) increases rapidly with decreasing temperature. This behaviour is similar to many other iron-based superconductors, but, more unusually, this sample then transforms back to tetragonal

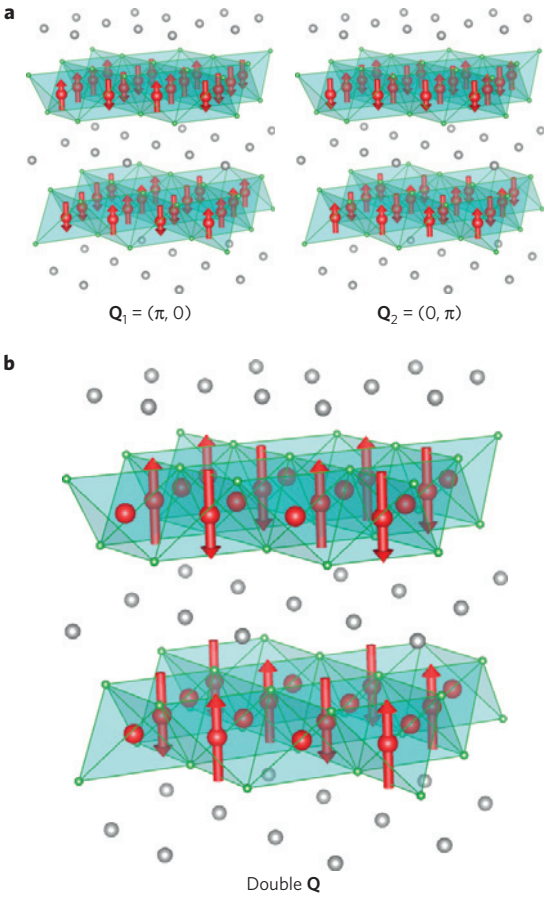

Figure 2 | Single-Q and double-Q magnetic models. a, Single-**Q** model, in which spins are modulated with either $\mathbf{Q}_1 = (\pi, 0)$ or $\mathbf{Q}_2 = (0, \pi)$, parallel to the a and b axes, respectively, in different domains. **b**, Double-**Q** model, which is formed from the superposition of modulations along $\mathbf{Q}_1$ and $\mathbf{Q}_2$.

symmetry at a strongly first-order transition at $T_r \approx 73$ K. The first-order nature of this transition from C_2 to C_4 symmetry can be seen in Fig. 1b, which shows that the two phases coexist for ∼10 K below T_r.

Powder neutron diffraction confirms that both the C_2 and C_4 phases are magnetically ordered. Both the $(\frac{1}{2}\frac{1}{2}1)$ and $(\frac{1}{2}\frac{1}{2}3)$ magnetic peaks are present below T_N (Fig. 1c,d), but the increase in intensity of the former at T_r shows that there is a significant spin reorientation in the C_4 phase, as observed in $Ba_{1-x}Na_xFe_2As_2$ ($0.24 \leq x \leq 0.28$) (ref. 23). Because the transformation back to tetragonal symmetry is complete in $Sr_{0.63}Na_{0.37}Fe_2As_2$ below 60 K, we are able to obtain a more reliable refinement of the magnetic structure than was possible in the earlier work. Figure 1e shows that the data can be fitted well by a model with moments along c-axis, in agreement with the moment direction deduced by Waßer and colleagues[35].

The magnetic Bragg peaks in the C_4 phase have the same reciprocal lattice indices as the C_2 phase, using the tetragonal unit cell, so one possible interpretation of the data is that the two phases have identical magnetic stripe order, differing only by the orientation of the iron spins. In this single-**Q** model, Bragg peaks from stripes parallel to the x and y axes in different domains would be incoherently superposed (Fig. 2a). Such a model would be magnetically orthorhombic, so magnetoelastic coupling should generate an orthorhombic structural distortion as well, but it is plausible that it is much weaker because of the spin reorientation, and therefore difficult to resolve.

An alternative interpretation is that there is a single domain comprising a coherent superposition of magnetic stripes parallel to

both the x and y axes, a double-**Q** model (Fig. 2b). This is the model predicted by itinerant approaches, in which magnetic order in the C_4 phase is generated by band nesting along the x and y directions simultaneously, restoring tetragonal symmetry[23]. In such a case, the residual spin–orbit coupling allows the parallel orientation of the resulting magnetic moments from each wavevector only if they are along the z-direction. It is well known that diffraction alone is unable to distinguish between multi-domain single-**Q** and single-domain multi-**Q** structures, as they produce identical Bragg peak intensities. As discussed in ref. 28, it might be possible to distinguish them with resonant X-ray scattering, which is sensitive to the orbital configuration of the iron d-electrons. In particular, space groups compatible with any possible d_{xz}/d_{yz} orbital order would be incompatible with a double-**Q** model.

Mössbauer spectroscopy. Although in reciprocal space, the single-**Q** and double-**Q** models look identical, they are remarkably different in real space. As shown in Fig. 2b, the coherent superposition of the orthogonal stripes in the double-**Q** model results in a doubling of the magnetic moments on half of the sites and a complete cancellation of the magnetic moments on the other half. That is, half of the iron sites are spin-density wave nodes. In local-moment systems, nodes represent fluctuating spins that have a high entropy, but, in an itinerant spin-density wave, they can be a natural consequence of a spatially inhomogeneous magnetization.

The best way to distinguish these two magnetic structures is therefore to use a local probe of the magnetization. Mössbauer spectroscopy is ideal because the Zeeman splitting of the nuclear levels of ^{57}Fe atoms is directly proportional to the static magnetization density at the nuclear site. Earlier Mössbauer spectra on iron arsenides were consistent with the temperature dependence of the conventional antiferromagnetic stripe order, which is characterized by a single hyperfine field at each temperature[40,41].

We have measured Mössbauer spectra at temperatures between 5 K and 125 K (Fig. 3). The 125 K spectrum shows, as expected, a single peak associated with the paramagnetic phase, with a small isomer shift due to the chemical environment that is independent of temperature. Spectra measured in the C_2 phase at 95, 85 and 75 K (only 85 K is shown) are well fitted with a single hyperfine field, characteristic of a single magnetic site, which grows with decreasing temperature (Fig. 3e). However, well below the C_4 transition, at 30 K, there is a qualitatively different spectrum, which consists of a large central peak with the same isomer shift as the paramagnetic phase, indicating the presence of non-magnetic sites, and a sextet indicating magnetic sites with a significantly larger effective field than in the C_2 phase (by a factor of ∼2). A free fit to such a two-site model shows that the spectral weights of each component are identical within the statistical uncertainty. In other words, 50% of the sites are magnetic and 50% are non-magnetic, exactly as predicted by the double-**Q** model.

The 65 K spectrum, which was taken in the temperature range where diffraction data indicated a coexistence of the C_4 and C_2 phases, shows evidence of the superposition of three components, two magnetic and one non-magnetic. Although the parameters are too highly correlated to be fit independently, the spectrum is consistent with a C_4 contribution, comprising an equal concentration of large moment and non-magnetic sites, and a C_2 contribution from smaller moment sites. Another parameter, the quadrupole splitting, which is sensitive to the point-group symmetry of the surrounding ions, changes sign between the C_2 and C_4 phases, but is otherwise nearly temperature independent. The resulting local magnetization of the magnetic sites as a function of temperature (Fig. 3e) shows a clear doubling of the magnetic moment within the C_4 phase compared to the C_2 phase, demonstrating that the C_4 magnetic structure involves a redistribution of magnetization density from the non-magnetic to the magnetic sites, an effect that is a clear fingerprint of an itinerant spin-density wave.

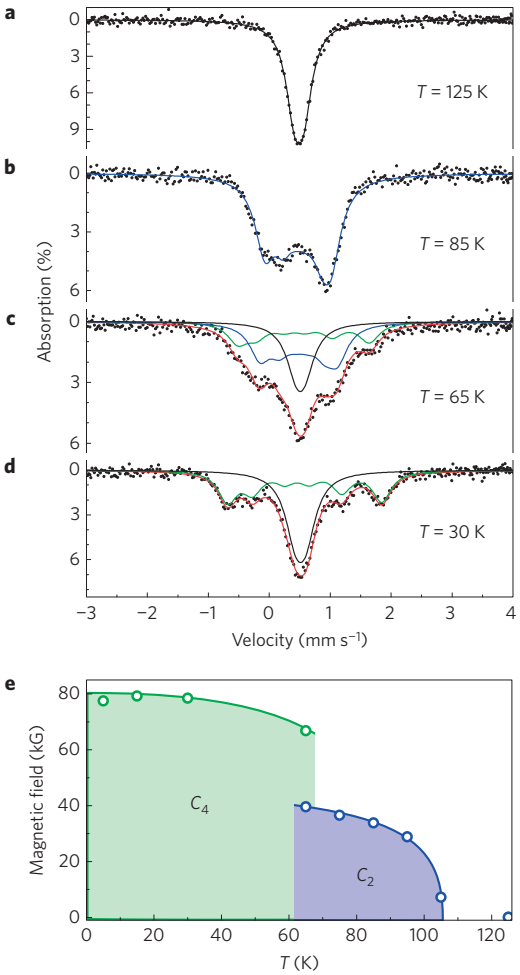

Figure 3 | Mössbauer spectroscopy data. a–d, Mössbauer spectra (black dots) at 30, 65, 85 and 125 K (5, 15, 75, 95 and 105 K not shown), respectively. Fits to the contributions of different iron sites are shown separately: non-magnetic sites (black lines), C_4 magnetic sites (green lines), C_2 magnetic sites (blue lines), total spectrum (red lines). **e**, Effective magnetic field on each magnetic site as a function of temperature as determined from Mössbauer spectroscopy. The lines are guides to the eye. Error bars are smaller than the points.

Discussion and conclusion

The Mössbauer data provide unambiguous evidence that the magnetism in the C_4 phase is a double-**Q** spin-density wave. This has a number of important consequences. As pointed out in ref. 28, such a double-**Q** magnetic structure is incompatible with either ferro-orbital order involving the d_{xz} and d_{yz} iron orbitals or with more complex patterns of orbital ordering. As a result, it implies that the nematic phase observed in the underdoped compounds is not the cause, but a consequence of magnetism, in agreement with the spin-nematic scenario[42]. Although this observation by itself cannot rule out the existence of orbital fluctuations, which favour the more conventional s-wave superconducting state, it does indicate the primary role played by magnetic fluctuations, which favour the unconventional sign-changing extended s-wave state.

The most important conclusion to be drawn from this work is that the nature of the C_4 magnetic state is not consistent with a model of localized spins on the iron sites, in which every iron site is magnetic. At least within the t-J_1-J_2 model, widely employed as an

effective model to study these materials[8,43,44], such a non-uniform magnetization is not a ground state of the model. It remains to be seen whether modifications of this model, with the inclusion of non-Heisenberg exchange interactions, such as the biquadratic or ring exchanges, could describe the non-uniform state.

By contrast, an itinerant approach offers a natural explanation of this non-uniform magnetic structure as the interference of two nesting-related spin-density waves, $\mathbf{S}(\mathbf{r}) = \mathbf{M}_1 \cos(\mathbf{Q}_1 \cdot \mathbf{r}) + \mathbf{M}_2 \cos(\mathbf{Q}_2 \cdot \mathbf{r})$, with $\mathbf{M}_1$ and $\mathbf{M}_2$ parallel to each other. The fact that $M_1 = M_2$ ensures not only the tetragonal symmetry of the system, in agreement with the experimental observations, but also implies that half of the sites are non-magnetic, with their spin density transferred to neighbouring sites with double the magnetization. This is a remarkable observation that is compatible only with itinerant band electrons. Furthermore, a secondary chequerboard charge order should accompany this non-uniform phase, in which the non-magnetic sites have locally a different charge density than the magnetic sites[34]. It has been argued that fluctuations of this secondary charge order can enhance the extended *s*-wave transition temperature[34].

The reorientation of the magnetization along the *c*-axis follows from general group-theory arguments related to the space group of a single FeAs plane with preserved tetragonal symmetry[45]. In the iron pnictides, spin–orbit coupling is not small[46] and, as a consequence, possible spin orientations are restricted to certain crystallographic directions. In particular, a group-theory analysis reveals three possibilities: $\mathbf{M}_1 \parallel \hat{\mathbf{x}}$ and $\mathbf{M}_2 \parallel \hat{\mathbf{y}}$; $\mathbf{M}_1 \parallel \hat{\mathbf{y}}$ and $\mathbf{M}_2 \parallel \hat{\mathbf{x}}$; or $\mathbf{M}_1 \parallel \hat{\mathbf{z}}$ and $\mathbf{M}_2 \parallel \hat{\mathbf{z}}$ (ref. 47). Because only the latter is compatible with the non-uniform state discussed here, the spins must point along the *c*-axis. This is discussed in more detail in the Supplementary Information.

Although weak-coupling itinerant models have indeed predicted a collinear double-**Q** state[23,29,31–33], our observations do not imply that the correlations in the iron pnictides are necessarily weak. Indeed, even in a well-known itinerant magnet such as elemental iron, a weak-coupling approach does not fully describe the properties of the ferromagnetic state[4]. In the iron pnictides, electron interactions were shown to be important to capture high-energy properties of the spin spectrum[19] and the sizeable fluctuating moment observed in the paramagnetic state[17]. Furthermore, because correlations induced by the Hund's rule coupling affect distinct Fe orbitals differently[9,19,20], hybrid models containing both localized and itinerant spins have been proposed[18,21]. It will be interesting to investigate the onset of the collinear double-**Q** state within such models.

Besides providing unambiguous evidence for the itinerant character of the magnetic order in the iron pnictides, highlighting the importance of longitudinal spin fluctuations, our work unveils a rare example of a collinear commensurate double-**Q** state. This contrasts with previous reports of multiple-**Q** order in itinerant systems, which involved non-collinear structures[36–38]. Unveiling the microscopic mechanisms responsible for this rather unique behaviour may offer important insights into the superconducting state of the iron pnictides, which appears in close proximity to this double-**Q** phase.

Methods

Methods and any associated references are available in the online version of the paper.

Received 26 May 2015; accepted 4 December 2015; published online 25 January 2016

References

1. Slater, J. C. Ferromagnetism and the band theory. *Rev. Mod. Phys.* **25**, 199–210 (1953).
2. Van Vleck, J. H. Models of exchange coupling in ferromagnetic media. *Rev. Mod. Phys.* **25**, 220–227 (1953).
3. Herring, C. in *Magnetism* (eds Rado, G. T. & Suhl, H.) Vol. IV (Academic, 1966).
4. Moriya, T. & Takahashi, Y. Itinerant electron magnetism. *Annu. Rev. Mater. Sci.* **14**, 1–25 (1984).
5. Chubukov, A. V. Pairing mechanism in Fe-based superconductors. *Annu. Rev. Condens. Matter Phys.* **3**, 57–92 (2012).
6. Hirschfeld, P. J., Korshunov, M. M. & Mazin, I. I. Gap symmetry and structure of Fe-based superconductors. *Rep. Prog. Phys.* **74**, 124508 (2011).
7. Si, Q. & Abrahams, E. Strong correlations and magnetic frustration in the high T_c iron pnictides. *Phys. Rev. Lett.* **101**, 076401 (2008).
8. Seo, K., Bernevig, B. A. & Hu, J. Pairing symmetry in a two-orbital exchange coupling model of oxypnictides. *Phys. Rev. Lett.* **101**, 206404 (2008).
9. de' Medici, L., Giovannetti, G. & Capone, M. Selective Mott physics as a key to iron superconductors. *Phys. Rev. Lett.* **112**, 177001 (2014).
10. Krüger, F., Kumar, S., Zaanen, J. & van den Brink, J. Spin-orbital frustrations and anomalous metallic state in iron-pnictide superconductors. *Phys. Rev. B* **79**, 054504 (2009).
11. Kontani, H., Inoue, Y., Saito, T., Yamakawa, Y. & Onari, S. Orbital fluctuation theory in iron-based superconductors: s^{++}-wave superconductivity, structure transition, and impurity-induced nematic order. *Solid State Commun.* **152**, 718–727 (2012).
12. Chubukov, A. V., Efremov, D. V. & Eremin, I. Magnetism, superconductivity, and pairing symmetry in iron-based superconductors. *Phys. Rev. B* **78**, 134512 (2008).
13. Cvetkovic, V. & Tešanović, Z. Multiband magnetism and superconductivity in Fe-based compounds. *Europhys. Lett.* **85**, 37002 (2009).
14. Fernandes, R. M. *et al*. Unconventional pairing in the iron arsenide superconductors. *Phys. Rev. B* **81**, 140501 (2010).
15. Fernandes, R. M., Chubukov, A. V. & Schmalian, J. What drives nematic order in iron-based superconductors? *Nature Phys.* **10**, 97–104 (2014).
16. Johannes, M. & Mazin, I. Microscopic origin of magnetism and magnetic interactions in ferropnictides. *Phys. Rev. B* **79**, 220510 (2009).
17. Hansmann, P. *et al*. Dichotomy between large local and small ordered magnetic moments in iron-based superconductors. *Phys. Rev. Lett.* **104**, 197002 (2010).
18. Yin, W.-G., Lee, C.-C. & Ku, W. Unified picture for magnetic correlations in iron-based superconductors. *Phys. Rev. Lett.* **105**, 107004 (2010).
19. Yin, Z. P., Haule, K. & Kotliar, G. Kinetic frustration and the nature of the magnetic and paramagnetic states in iron pnictides and iron chalcogenides. *Nature Mater.* **10**, 932–935 (2011).
20. Bascones, E., Valenzuela, B. & Calderón, M. J. Orbital differentiation and the role of orbital ordering in the magnetic state of Fe superconductors. *Phys. Rev. B* **86**, 174508 (2012).
21. Dai, P., Hu, J. & Dagotto, E. Magnetism and its microscopic origin in iron-based high-temperature superconductors. *Nature Phys.* **8**, 709–718 (2012).
22. Avci, S. *et al*. Structural, magnetic, and superconducting properties of $Ba_{1-x}Na_xFe_2As_2$. *Phys. Rev. B* **88**, 094510 (2013).
23. Avci, S. *et al*. Magnetically driven suppression of nematic order in an iron-based superconductor. *Nature Commun.* **5**, 3845 (2014).
24. Yu, R., Goswami, P., Si, Q., Nikolic, P. & Zhu, J.-X. Superconductivity at the border of electron localization and itinerancy. *Nature Commun.* **4**, 2783 (2013).
25. Böhmer, A. E. *et al*. Superconductivity-induced re-entrance of the orthorhombic distortion in $Ba_{1-x}K_xFe_2As_2$. *Nature Commun.* **6**, 7911 (2015).
26. Allred, J. M. *et al*. Tetragonal magnetic phase in $Ba_{1-x}K_xFe_2As_2$ from X-ray and neutron diffraction. *Phys. Rev. B* **92**, 094515 (2015).
27. Hassinger, E. *et al*. Pressure-induced Fermi-surface reconstruction in the iron-arsenide superconductor $Ba_{1-x}K_xFe_2As_2$: evidence of a phase transition inside the antiferromagnetic phase. *Phys. Rev. B* **86**, 140502 (2012).
28. Khalyavin, D. D. *et al*. Symmetry of reentrant tetragonal phase in $Ba_{1-x}Na_xFe_2As_2$: magnetic versus orbital ordering mechanism. *Phys. Rev. B* **90**, 174511 (2014).
29. Giovannetti, G. *et al*. Proximity of iron pnictide superconductors to a quantum tricritical point. *Nature Commun.* **2**, 398 (2011).
30. Eremin, I. & Chubukov, A. V. Magnetic degeneracy and hidden metallicity of the spin-density-wave state in ferropnictides. *Phys. Rev. B* **81**, 024511 (2010).
31. Brydon, P. M. R., Schmiedt, J. & Timm, C. Microscopically derived Ginzburg-Landau theory for magnetic order in the iron pnictides. *Phys. Rev. B* **84**, 214510 (2011).
32. Wang, X., Kang, J. & Fernandes, R. M. Magnetic order without tetragonal-symmetry-breaking in iron arsenides: microscopic mechanism and spin-wave spectrum. *Phys. Rev. B* **91**, 024401 (2015).
33. Gastiasoro, M. N. & Andersen, B. M. Competing magnetic double-Q phases and superconductivity-induced re-entrance of C_2 magnetic stripe order in iron pnictides. *Phys. Rev. B* **92**, 140506 (2015).
34. Fernandes, R. M., Kivelson, S. A. & Berg, E. Is there a hidden chiral density-wave in the iron-based superconductors? Preprint at http://arXiv.org/abs/1504.03656 (2015).

35. Waßer, F. *et al*. Spin reorientation in $Ba_{0.65}Na_{0.35}Fe_2As_2$ studied by single-crystal neutron diffraction. *Phys. Rev. B* **91**, 060505 (2015).
36. Jo, T. On the possibility of the multiple spin density wave state in the first-kind antiferromagnetic FCC metals. *J. Phys. F* **13**, L211–L216 (1983).
37. Long, M. W. Effects that can stabilise multiple spin-density waves. *J. Phys. Condens. Matter* **1**, 2857–2874 (1989).
38. Fishman, R. S. *et al*. Structural and magnetic phase transitions in Mn–Ni alloys. *Phys. Rev. B* **61**, 12159–12168 (2000).
39. Cortes-Gil, R. & Clarke, S. J. Structure, magnetism, and superconductivity of the layered iron arsenides $Sr_{1-x}Na_xFe_2As_2$. *Chem. Mater.* **23**, 1009–1016 (2011).
40. McGuire, M. A. *et al*. Phase transitions in LaFeAsO: structural, magnetic, elastic, and transport properties, heat capacity and Mössbauer spectra. *Phys. Rev. B* **78**, 094517 (2008).
41. Kitao, S. *et al*. Spin ordering in LaFeAsO and its suppression in superconductor $LaFeAsO_{0.89}F_{0.11}$ probed by Mössbauer spectroscopy. *J. Phys. Soc. Jpn* **77**, 103706 (2008).
42. Fernandes, R. M., Chubukov, A. V., Knolle, J., Eremin, I. & Schmalian, J. Preemptive nematic order, pseudogap, and orbital order in the iron pnictides. *Phys. Rev. B* **85**, 024534 (2012).
43. Lv, W., Wu, J. & Phillips, P. W. Orbital ordering induces structural phase transition and the resistivity anomaly in iron pnictides. *Phys. Rev. B* **80**, 224506 (2009).
44. Yu, R., Zhu, J.-X. & Si, Q. Orbital-selective superconductivity, gap anisotropy, and spin resonance excitations in a multiorbital t-J_1-J_2 model for iron pnictides. *Phys. Rev. B* **89**, 024509 (2014).
45. Cvetkovic, V. & Vafek, O. Space group symmetry, spin–orbit coupling, and the low-energy effective Hamiltonian for iron-based superconductors. *Phys. Rev. B* **88**, 134510 (2013).
46. Borisenko, S. V. *et al*. Direct observation of spin–orbit coupling in iron-based superconductors. *Nature Phys.* http://dx.doi.org/10.1038/nphys3594 (2015).
47. Christensen, M. H., Kang, J., Andersen, B. M., Eremin, I. & Fernandes, R. M. Spin reorientation driven by the interplay between spin–orbit coupling and Hund's rule coupling in iron pnictides. *Phys. Rev. B* **92**, 214509 (2015).

Acknowledgements

Work at Argonne (J.M.A., K.M.T., D.E.Bugaris, M.J.K., D.Y.C., H.C., M.G.K., S.R., O.C. and R.O.) was supported by the US Department of Energy, Office of Science, Materials Science and Engineering Division. X-ray experiments were performed at the Advanced Photon Source, which is supported by the Office of Basic Energy Sciences under Contract No. DE-AC02-06CH11357. Neutron experiments were performed at the High Flux Isotope Reactor and Spallation Neutron Source. R.M.F. and J.K. were supported by the US Department of Energy, Office of Science, Basic Energy Sciences, under award number DE-SC0012336. The work of I.E. was supported by the Focus Program 1458 Eisen-Pniktide of the DFG, and by the German Academic Exchange Service (DAAD PPP USA no. 57051534). I.E. also acknowledges the financial support of the Ministry of Education and Science of the Russian Federation in the framework of Increase Competitiveness Program of NUST MISiS (N 22014015). The authors thank A. A. Aczel, A. Huq, M. J. Kirkham and P. S. Whitfield for experimental assistance, E. E. Alp for use of his Mössbauer spectrometer, and B. M. Andersen, A. V. Chubukov, M. N. Gastiasoro, A. Yaresko and Y. Zhao for fruitful discussions.

Author contributions

Samples were prepared by D.E.Bugaris, with additional support from D.Y.C., and M.G.K. The experiments were devised by J.M.A., K.M.T., O.C., S.R. and R.O. The X-ray and neutron diffraction experiments were performed by J.M.A., K.M.T., O.C., M.J.K., S.R. and S.H.L. Mössbauer spectroscopy was performed by D.E.Brown Magnetization measurements were performed by H.C. The data were analysed by J.M.A., K.M.T., O.C., S.R., R.O. and D.E.Brown. Theoretical interpretation was provided by J.K., R.M.F. and I.E. The manuscript and Supplementary Information were written by J.M.A., R.O., R.M.F. and I.E. with input from all the authors.

Additional information

Supplementary information is available in the online version of the paper. Reprints and permissions information is available online at www.nature.com/reprints. Correspondence and requests for materials should be addressed to J.M.A.

Competing financial interests

The authors declare no competing financial interests.

Methods

Synthesis. Handling of all starting materials was performed in an M-Braun glovebox under an inert Ar atmosphere (<0.1 ppm of H_2O and O_2). Sr (Aldrich, 99.9%) and Fe (Alfa Aesar, 99.99+%) were used as received. Small pieces of Na, free of oxide coating, were trimmed from large lumps (Aldrich, 99%). Granules of As (Alfa Aesar, 99.99999+%) were ground to a coarse powder before use. The precursor materials SrAs, NaAs and Fe_2As were synthesized in quartz tubes from stoichiometric reactions of the elements at 800 °C, 350 °C and 700 °C, respectively. Polycrystalline samples of $Sr_{0.67}Na_{0.37}Fe_2As_2$ were prepared from stoichiometric mixtures of SrAs, NaAs and Fe_2As, which were ground thoroughly with a mortar and pestle, and loaded in alumina crucibles. The alumina crucibles were sealed in Nb tubes under Ar, which were further sealed in quartz tubes under vacuum. The reaction mixtures were subjected to multiple heating cycles between 850 and 950 °C for durations less than 48 h (to minimize loss of Na by volatilization). The samples underwent grinding by mortar and pestle between heating cycles to homogenize the compositions. Following the final heating cycles, the sealed samples were quenched in air from the maximum temperature rather than allowing them to cool slowly. Initial characterization of the dark grey powders was conducted by laboratory powder X-ray diffraction and magnetization measurements. More details of the sample characterization are provided in the Supplementary Information.

Powder diffraction. X-ray powder diffraction measurements were performed at Argonne National Laboratory using beamline 11-BM at the Advanced Photon Source. Neutron powder diffraction measurements were performed at Oak Ridge National Laboratory using beamline HB-1A at the High Flux Isotope Reactor and the POWGEN diffractometer at the Spallation Neutron Source.

Mössbauer spectroscopy. Mössbauer measurements were performed in transmission geometry with a sinusoidally driven 2 mCi ^{57}Co(Rh) source and a germanium detector. Silicon diode sensors allowed the control and stabilization of the sample temperature to within 0.2 K for a conventional bath cryostat. The sample studied had an area density of (4×0.02) mg cm^{-2} of ^{57}Fe and was placed on a 99.999% pure aluminium foil held in place by kapton tape. This effectively thin sample yielded a linewidth of 0.34 mm s^{-1} at 125 K (where the sample is in the paramagnetic state), thus showing that the environment around the iron atoms is fairly uniform throughout the sample. Calibrations were made using a natural α-Fe foil. The spectra were fitted by varying the isomer shift, magnetic hyperfine field, and the electric quadrupole factor. The intensities of the magnetic sextet-split lines were constrained to a 1:2:3 ratio according to their Clebsch–Gordon coefficients (or magnetic dipole matrix elements), and the Lorentzian linewidths for all lines of a particular iron site were constrained to be the same. Details of the fit parameters are given in the Supplementary Information.